JOURNAL OF MAGNETIC RESONANCE **132,** 41–53 (1998)
ARTICLE NO. MN981397

# Evaluation of 3D NMR Experiments for the Characterization of Polymer Structure

Takeshi Saito and Peter L. Rinaldi[1]

*Department of Chemistry, Knight Chemical Laboratory, University of Akron, Akron, Ohio 44325-3601*

Received October 6, 1997

**A series of three-dimensional (3D) nuclear magnetic resonance (NMR) pulse sequences, utilizing pulsed-field gradient (PFG) techniques, were developed or adapted from biological experiments for applications in the characterization of polymer structure. These experiments form the foundation of a suite of experiments which can be used to characterize the structure of polymers and other heteroatom-containing organic materials, in much the same way that the data from multiple 3D NMR experiments have been used in biological structure determination. Several variations of an $^{1}H/X/Y$ chemical shift correlation (HXY) experiment are exhibited, and the HCX sequence (where Y = $^{13}C$) is combined with $^{13}C$ homonuclear isotropic mixing to generate new pulse sequences which provide additional structural information. In this paper, the spectra of poly($\alpha,\beta$-$^{13}C_2$-styrene) (PS) prepared by diphenylphosphinyl radical (DPPR) initiated polymerization of $\alpha,\beta$-$^{13}C_2$-styrene are used to illustrate the application of these techniques for characterization of polymer chain end structures. Comments on the relative advantages of the pulse sequence are provided. Although polymers are used to illustrate the applications of these pulse sequences, the sequences can just as easily be used to study other organic structures containing an NMR-active X nucleus. Organometallic chemistry is especially suited for applications of these NMR experiments.** 

*Key Words:* **3D NMR; triple resonance NMR; polystyrene; $^{13}C$-labeling.**

## INTRODUCTION

Nuclear magnetic resonance (NMR) has been a powerful tool for the analysis of polymer microstructures and polymer chain end groups. Much of this work has involved $^{13}C$ NMR. Two of the major limitations of chain end analysis of polymers are the low concentration of the chain end groups in the polymer and interference from overlapping resonances. One common approach to overcoming the former problem is to use $^{13}C$ enriched initiators (*1–3*), which enhance the signals originating from the initiator fragments relative to those of the main chain repeat units. When 100% $^{13}C$ enrichment is used, signals originating from the chain ends often have intensities which are comparable to those originating from the polymer backbone. One drawback of this technique involves the interference from overlap with extremely intense signals of the polymer backbone. These signals often interfere with detection of the weak chain end signals of interest.

To resolve this problem, utilization of a third NMR-active nucleus can often be useful. This can be accomplished by artificial enrichment or by utilizing an X nucleus such as $^{31}P$ or $^{19}F$ (100% natural abundance) which is already present in the structure. In favorable cases, direct observation of this third nucleus provides a spectrum with very large chemical shift dispersion and only a few resonances (when there are a limited number of X atoms in the molecule). The idea of using isotopic labeling together with triple resonance NMR techniques to selectively observe resonances from the label site, while filtering the remainder of the signals from the spectrum, was described in 1982 (*4, 5*).

Recently, triple resonance experiments have taken the form of three-dimensional (3D) NMR and have been used in conjunction with isotopic labeling to study the structures of biological macromolecules. The HNCO experiment was originally developed by Bax *et al.* (*6, 7*) to help determine the structures of $^{13}C$- and $^{15}N$-labeled proteins. Later, Berger adapted the HNCO experiment to the $^{1}H/^{13}C/^{31}P$ spin system (*8, 9*) in order to obtain unambiguous resonance assignments of organometallic compounds. Others described the use of the HNCO experiment for the determination of RNA structures (*10, 11*). By using the chemical shift dispersion of the $^{31}P$ nuclei, these experiments spread overlapping $^{1}H$ and $^{13}C$ resonances, and thus permitted the resolution and assignment of resonances from complex molecules.

Since the development of these techniques, many variations of 3D NMR pulse sequences have been described. Suites of experiments have been designed so that when several of these are used together, the entire 3D solution structure of a protein can be determined (*12*). When 3D triple resonance methods are combined with pulsed-field gradient (PFG) techniques (*13*), artifact-free spectra can

[1] To whom correspondence should be addressed. E-mail: PeterRinaldi@uakron.edu. Fax: 330-972-5256.



1090-7807/98 $25.00

be obtained in a short time. Combination of these modern NMR techniques provides tremendously enhanced methods for detection of resonances from minor structures such as polymer chain ends without interference from the intense signals of components which are present in significantly higher abundance (*14*).

Development of 3D NMR methods for applications in polymer science offers the potential of tremendously improving our ability to study polymer structures, with a concomitant improvement in our understanding of polymer-forming reactions. However, applications of solution 3D NMR methods in polymer science have been rare. In this paper, we describe a suite of 3D NMR experiments which have been adapted for use in the study of polymer microstructure. Resonances from selected fragments such as chain ends, branches, defects, block junctions, and graft points can be detected without interference from the remaining signals of the polymer. Here, the use of various HXY, chemical shift correlation, 3D NMR experiments (where Y = $^{13}$C and X = $^{31}$P) to characterize polymer chain end structures is presented. Applications of these methods are illustrated with 3D NMR spectra of the phosphorus-containing chain-end structures in polystyrene (PS) and poly($\alpha$,$\beta$-$^{13}C_2$-styrene) prepared by initiation of styrene polymerization using diphenylphosphinyl radical (DPPR). The methods are compared and their relative advantages are discussed.

## EXPERIMENTAL

All NMR spectra were obtained on a Varian Unity*plus* 600-MHz spectrometer equipped with Ultra·shims, a PFG accessory, and a Nalorac 5-mm $^1$H/$^{13}$C/X PFG triple resonance probe (where X can be tuned to frequencies between the resonances of $^{31}$P and $^{15}$N nuclei). The samples consisted of 110 mg of DPPR initiated PS in 0.7 mL $CDCl_3$ for the natural abundance polystyrene and 34 mg of DPPR initiated PS-$^{13}C_2$ in 0.7 mL $C_6D_6$ for experiments requiring $^{13}$C-enriched polystyrene. The temperature was regulated at 30.0 ± 0.1°C. All data processing was performed on a Sun SPARCstation 10 using Varian's Vnmr software. All the 3D data were processed with a combination of shifted sinebell and Gaussian weighting in all dimensions. 3D Fourier transforms were performed on 256 × 256 × 256 matrices. The preparation of polystyrene samples has been described elsewhere (*15*).

### *2D $^1$H–$^{13}$C HMQC Experiment*

The following parameters were used in the $^1$H–$^{13}$C PFG–HMQC experiment: $^1$H and $^{13}$C 90° pulse widths of 10.8 and 20.0 $\mu$s, respectively; 28469.8 and 5926.8 Hz spectral windows in the $^{13}$C ($f_1$) and $^1$H ($f_2$) dimensions, respectively; four transients for each of 1024 real $t_1$ increments; a 1.0-s relaxation delay; and a 0.049-s acquisition time with $^{13}$C GARP-1 (*16*) decoupling with a field strength of 3.91 kHz. The delay, $\Delta$, was optimized for $(2^1J_{HC})^{-1}$ = 3.22 ms. The strengths of the three 2.0-ms PFGs were gl = 0.191, g2 = 0.191, and g3 = −0.0960 Tm$^{-1}$, respectively. The data were processed with sinebell weighting; and the spectrum was displayed in the magnitude mode in both dimensions. 2D FT was performed on a 1024 × 1024 matrix.

### *3D MQ-HCAP Experiment*

The following parameters were used with the pulse sequence shown in Fig. 1a to obtain the MQ-HCAP 3D NMR spectrum: $^1$H, $^{13}$C, and $^{31}$P 90° pulse widths of 10.0, 20.0, and 15.0 $\mu$s, respectively; 2344.0, 2433.5, and 1339.6 Hz spectral windows in the $^{13}$C ($f_1$), $^{31}$P ($f_2$), and $^1$H ($f_3$) dimensions, respectively; four transients for each of the 64 complex $t_1$ and 32 complex $t_2$ increments; a 1.5-s relaxation delay; and a 0.049-s acquisition time with simultaneous $^{13}$C and $^{31}$P GARP-1 decoupling with field strengths of 3.91 and 5.06 kHz, respectively, during the acquisition time. The delays were optimized to $\Delta = (4^1J_{HC})^{-1}$ = 1.78 ms, and $\tau = (4^1J_{CP})^{-1}$ = 4.17 ms. PFGs g1 and g2 were applied for 2.0 and 1.0 ms with strengths of 0.243 and 0.122 Tm$^{-1}$, respectively. These PFGs provide coherence selection between $^{13}$C and $^1$H nuclei. The total experiment time was about 17 h. Digital signal processing (DSP) was applied to reduce a spectral window in $f_3$ from 1339.6 to 598.4 Hz.

### *3D SQ-HCAP Experiment*

The following parameters were used with the pulse sequence shown in Fig. 1b to obtain the SQ-HCAP 3D NMR spectrum; $^1$H, $^{13}$C, and $^{31}$P 90° pulse widths of 11.2, 20.0, and 15.0 $\mu$s, respectively; 2433.5, 2344.0, and 1339.6 Hz spectral windows in the $^{31}$P ($f_1$), $^{13}$C ($f_2$), and $^1$H ($f_3$) dimensions; four transients for each of the 32 complex $t_1$ and 64 complex $t_2$ increments; a 1.5-s relaxation delay; and a 0.053-s acquisition time with $^{13}$C GARP-1 decoupling with field strength of 3.91 kHz. The delays were set to $\Delta = (4^1J_{HC})^{-1}$ = 1.78 ms and $\tau = (4^1J_{CP})^{-1}$ = 4.17 ms. Gradients g1 and g2 were applied for 2.0 and 1.0 ms with strengths of 0.243 and 0.121 Tm$^{-1}$, respectively. These PFGs provide coherence selection between $^{13}$C and $^1$H nuclei. The total experiments time was about 17 h. DSP was applied to reduce a spectral window in $f_3$ from 1339.6 to 598.4 Hz.

### *3D CT-HCAP Experiment*

The following parameters were used with the pulse sequence shown in Fig. 1c to obtain the CT-HCAP 3D NMR spectrum: $^1$H, $^{13}$C, and $^{31}$P 90° pulse widths of 10.5, 20.0, and 17.0 $\mu$s, respectively; 606.2, 2556.9, and 8000.0 Hz spectral windows in the $^{31}$P ($f_1$), $^{13}$C ($f_2$), and $^1$H ($f_3$) dimensions, respectively; four transients for each of the 16 complex $t_1$ and 64 complex $t_2$ increments; a 1.0-s relaxation delay; and a 0.048-s acquisition time with $^{13}$C MPF7 (*17, 18*) de-

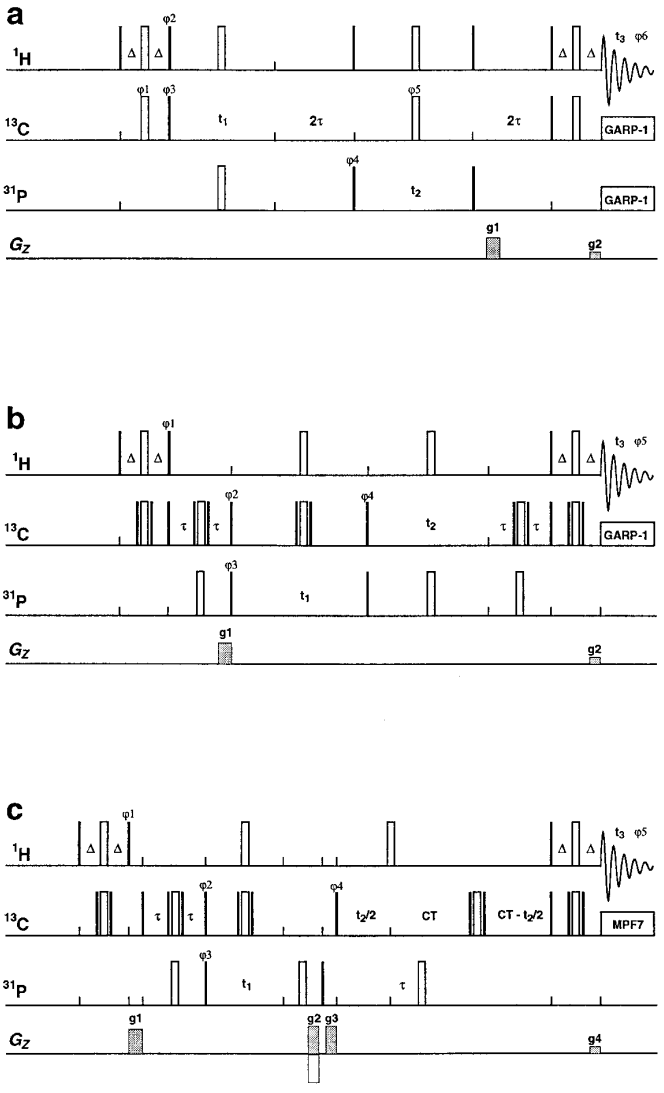


**FIG. 1.** Pulse sequence diagrams for: (a) MQ-HCAP, (b) SQ-HCAP, and (c) CT-HCAP experiments. Solid and open pulses are 90° and 180° pulses, respectively. The phase cycling is as follows: (a) $\varphi1 = x, -x$; $\varphi2 = y, -y$; $\varphi3 = x$ [incremented in $t_1$ according to the States method (*31*)]; $\varphi4 = x, -x, -x, x$ (incremented in $t_2$ according to the States method); $\varphi5 = 4(x), 4(y), 4(-x), 4(-y)$; $\varphi6 = x, 2(-x), x, -x, 2(x), -x$. All other pulses were applied along the $+x$-axis. (b) $\varphi1 = y$; $\varphi2 = y$; $\varphi3 = x, -x$ (incremented in $t_1$ according to the States method); $\varphi4 = 2y, 2(-y)$ (incremented in $t_2$ according to the States method); $\varphi5 = x, -x, -x, x$. All composite $^{13}$C pulses have relative phase of *x, y, x.* (c) $\varphi1 = y$; $\varphi2 = y$; $\varphi3 = x, -x$; $\varphi4 = 2y, 2(-y)$ incremented in $t_2$ according to the States method); $\varphi5 = x, -x, -x, x$. Two spectra were collected with different signs of the second PFG and combined to obtain pure absorption spectrum (*32*) in $f_1$.

coupling with a field strength of 2.49 kHz. The delays were set at $\Delta = (4\,^1J_{HC})^{-1} = 1.78$ ms, $\tau = (4\,^1J_{CP})^{-1} = 4.17$ ms, and $CT = (2\,^1J_{CC})^{-1} = 14.3$ ms, respectively. Gradients g1 through g4 were applied for 3.0, 1.0, 2.0, and 1.0 ms, with strengths of 0.247, 0.309, 0.309, and 0.125 $Tm^{-1}$, respectively. The second and fourth PFGs provide coherence selection between $^{31}$P and $^1$H nuclei, while the first and third PFGs were used for purging all undesired signals. The total experiment time was about 7.25 h. DSP was applied to reduce a spectral window in $f_3$ from 8000.0 to 2000.0 Hz. Linear prediction (LP) was used to forward extend the data in the $t_1$ and $t_2$ time dimensions to twice the original size (12 complex points were used to calculate 2 coefficients).

### *3D CT-HCBP Experiment*

The following parameters were used with the pulse sequence shown in Fig. 1c to obtain the long-range HCP (HCBP) 3D NMR spectrum: $^1$H, $^{13}$C, and $^{31}$P 90° pulse widths of 10.2, 20.0, and 17.0 $\mu$s, respectively; 606.2, 2556.9, and 8000.0 Hz spectral windows in the $^{31}$P ($f_1$), $^{13}$C ($f_2$), and $^1$H ($f_3$) dimensions, respectively; 4 transients for each of the 16 complex $t_1$ and 64 complex $t_2$ increments; a 1.0-s relaxation delay; and a 0.048-s acquisition time with $^{13}$C MPF7 decoupling with a field strength of 2.49 kHz. The delays were set at $\Delta = (4\,^1J_{HC})^{-1} = 1.78$ ms and $CT = \tau = (4\,^{LR}J_{CP})^{-1} = 16.7$ ms, respectively. Gradients g1 through g4 were applied for 3.0, 1.0, 2.0, and 1.0 ms, with strengths of 0.247, 0.309, 0.309, and 0.125 $Tm^{-1}$, respectively. The second and fourth PFGs provided coherence selection between $^{31}$P and $^1$H nuclei, while the first and third PFGs were used for purging all undesired signals. The total experiment time was about 7.5 h. DSP was applied to reduce a spectral window in $f_3$ from 8000.0 to 2000.0 Hz. LP was used to forward extend the data in the $t_1$ and $t_2$ time dimensions to twice the original size (12 complex points were used to calculate 2 coefficients).

### *3D H(CA)P–CC-TOCSY Experiment*

The following parameters were used with the pulse sequence shown in Fig. 2a to obtain the H(CA)P–CC-TOCSY 3D NMR spectrum: $^1$H, $^{13}$C, and $^{31}$P 90° pulse widths of 10.3, 20.0, and 17.0 $\mu$s, respectively; 606.2, 2556.9, and 8000.0 Hz spectral windows in the $^{31}$P ($f_1$), $^{13}$C ($f_2$), and $^1$H ($f_3$) dimensions, respectively; 16 transients for each of the 16 complex $t_1$ and 64 complex $t_2$ increments; a 1.0-s relaxation delay; a 0.048-s acquisition time with $^{13}$C MPF7 decoupling with a field strength of 2.49 kHz; a 10.4-ms isotropic mixing time using DIPSI-3 (*19*) sequence with a field strength of 5.21 kHz followed by a 2.0-ms trim pulse; $^1$H WALTZ-16 (*20*) decoupling with a field strength of 2.00 kHz was applied during the sequence. The delays were set to $\Delta = (4\,^1J_{HC})^{-1} = 1.78$ ms, $\delta = (6\,^1J_{HC})^{-1} = 1.19$ ms, $\tau = (4\,^1J_{CP})^{-1} = 4.17$ ms, and $CT = (2\,^1J_{CC})^{-1} = 14.3$ ms. Gradients g1 through g4 were applied for 3.0, 1.0, 2.0, and 1.0 ms with strengths of 0.247, 0.309, 0.309, and 0.125 $Tm^{-1}$, respectively. The second and fourth PFGs provide coherence selection between $^{31}$P and $^1$H nuclei, while the first and third PFGs were used for purging all undesired

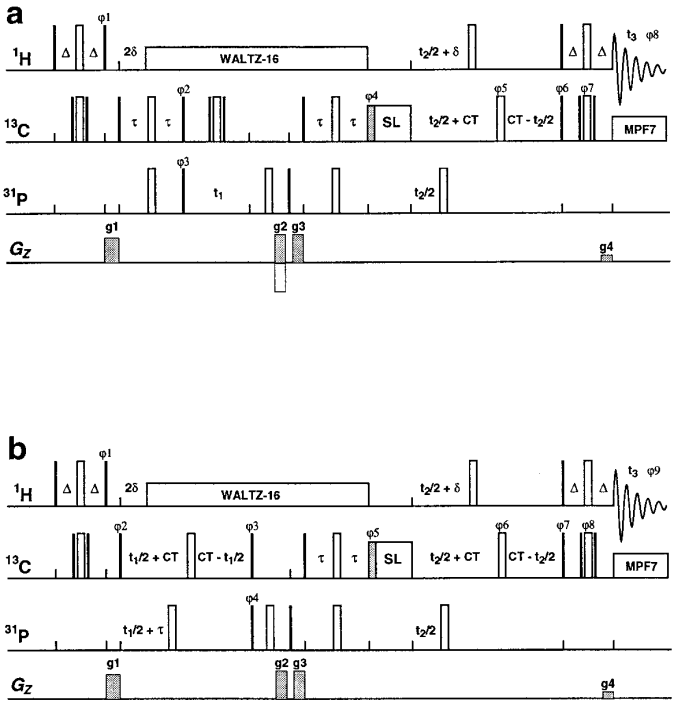


**FIG. 2.** Pulse sequence diagrams for $^{13}C$ homonuclear spin locking experiments: (a) H(CA)P–CC-TOCSY and (b) HCA(P)–CC-TOCSY. Solid and open pulses are 90° and 180° pulses, respectively. The phase cycling used is as follows: (a) $\varphi1 = y$; $\varphi2 = y$; $\varphi3 = x, -x$; $\varphi4 = 2y,2(-y)$ (incremented in $t_2$ according to the States method); $\varphi5 = x, -x, -x,x$. Two spectra were collected with different signs of the second PFG and combined to obtain a pure absorption spectrum in $f_1$. (b) $\varphi1 = y, -y$; $\varphi2 = x, -x$; $\varphi3 = 2x, 2(-x)$; $\varphi4 = 4x, 4(-x)$; $\varphi5 = 4x, 4y, 4(-x), 4(-y)$; $\varphi6 = x$ (incremented in $t_2$ according to the States method); $\varphi7 = 4x, 4(-x)$; $\varphi8 = 4x, 4(-x)$. Two spectra were collected with different signs of the second PFG and combined to obtain pure absorption spectrum in $f_1$.

signals. The total experiment time was about 25.25 h. DSP was applied to reduce a spectral window in $f_3$ from 8000.0 to 2000.0 Hz. LP was used to forward extend the data in the $t_1$ and $t_2$ time dimensions to twice the original size (12 complex points were used to calculate 2 coefficients).

### *3D HCA(P)–CC-TOCSY Experiment*

The following parameters were used with the pulse sequence shown in Fig. 2b to obtain the HCA(P)–CC-TOCSY 3D NMR spectrum: $^1H$, $^{13}C$, and $^{31}P$ 90° pulse widths of 10.3, 20.0, and 17.0 $\mu$s, respectively; 598.9, 2556.9, and 8000.0 Hz spectral windows in the $^{13}C$ (before the isotropic mixing, $f_1$), $^{13}C$ (after the isotropic mixing, $f_2$), and $^1H$ ($f_3$) dimensions, respectively; 16 transients for each of the 16 complex $t_1$ and 64 complex $t_2$ increments; a 1.0-s relaxation delay; a 0.048-s acquisition time with $^{13}C$ MPF7 decoupling using a field strength of 2.49 kHz; and a 10.4-ms isotropic mixing time using the DIPSI-3 sequence with a field strength of 5.21 kHz followed by a 2.0-ms trim pulse. The delays were set at $\Delta = (4^1J_{HC})^{-1} = 1.78$ ms, $\delta = (6^1J_{HC})^{-1} = 1.19$ ms, $\tau = (4^1J_{CP})^{-1} = 4.17$ ms, and CT $= (2^1J_{CC})^{-1} = 14.3$ ms. Gradients g1 through g4 were applied for 3.0, 1.0, 2.0, and 1.0 ms with strengths of 0.247, 0.309, 0.309, and 0.125 $Tm^{-1}$, respectively. The second and fourth PFGs provide coherence selection between $^{31}P$ and $^1H$ nuclei, thus filtering out all signals from the spectrum except the ones from $CH_n$ attached to $^{31}P$ atoms, while the first and third PFGs were used for purging all undesired signals. The total experiment time was about 25.5 h. DSP was applied to reduce a spectral window in $f_3$ from 8000.0 to 2000.0 Hz. LP was used to forward extend the data in the $t_1$ and $t_2$ time dimensions to twice the original size (12 complex points were used to calculate 2 coefficients).

### *3D CT-HCCH Experiment*

The following parameters were used in with the pulse sequence shown in Fig. 3 to obtain the CT-HCCH (*21–23*) 3D NMR spectrum: 90° $^1H$ and $^{13}C$ pulse widths of 10.3 and 20.0 $\mu$s, respectively; 3008.9, 3008.9, and 8000.0 Hz spectral windows in the $^{13}C$ SQ ($f_1$), DQ ($f_2$) and $^1H$ ($f_3$) dimensions, respectively; 4 transients for each of 36 complex $t_1$ and 38 complex $t_2$ increments; a 1.0-s relaxation delay; a 0.052-s acquisition time with $^{13}C$ MPF7 decoupling using a field strength of 2.49 kHz. Decoupling on the $^{31}P$ channel was applied throughout the experiment using the MPF7 decoupling sequence with a field strength of 1.86 kHz. The PFGs g1, g2, and g3 were applied for 3.0, 1.0, and 1.0 ms with strengths of 0.309, 0.309, and 0.155 T $m^{-1}$, respectively. The second and third PFGs provide coherence selection between $^{13}C$ DQ and $^1H$ nuclei, while the first PFG was used for purging undesired signals. The delays $\Delta$ and $\delta$ were optimized for $(4^1J_{HC})^{-1} = 1.78$ ms, and CT was set to $(4^1J_{CC})^{-1} = 6.25$ ms. The total experiment time was about 8.25 h. DSP was applied to reduce a spectral window in $f_3$ from 8000.0 to 2000.0 Hz. LP was used to forward extend the data in the $t_1$ and $t_2$ time dimensions to twice the original

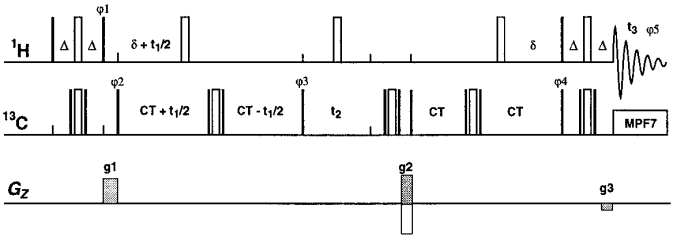


**FIG. 3.** Pulse sequence diagram for the CT-HCCH experiment. Solid and open pulses are 90° and 180° pulses, respectively. The phase cycling is as follows: $\varphi1 = y$; $\varphi2 = x$ (incremented in $t_1$ according to the States method); $\varphi3 = y$; $\varphi4 = y, -y$; $\varphi5 = x, -x$. Two spectra were collected with different signs of the second PFG and combined to obtain pure absorption spectrum in $f_2$.

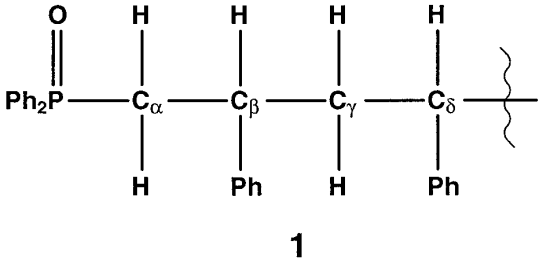


**1**

**SCHEME 1**

size (16 complex points were used to calculate 4 coefficients).

## RESULTS AND DISCUSSION

There are a number of possible chain end structures on PS, including structure **1,** which results from an initiation step that involves addition of a DPPR to the unsubstituted end of a styrene double bond. All discussions in this manuscript are restricted to the sections of the spectra which contain resonances from **1,** which is expected to be one of the predominant chain end structures in the sample. Of course, configurational isomers of this structure are also present because meso and racemic configurations of styrene–styrene enchainments near the chain end exist. The NMR spectra of the polymer may contain contributions from all of these and several other structures.

In biological NMR, the naming of pulse sequences is often established by connecting symbols for the fragments whose resonances are correlated in the spectrum. For example, the HNCA sequence (*6, 7*) is used to correlate the $^{1}H$, $^{15}N$, and $^{13}C_{\alpha}$ resonances of attached atoms within peptide amino acid residues. When an experiment involves coherence transfer through an atom whose chemical shift is not encoded during one of the evolution times, that fragment's symbol is enclosed by parentheses in the pulse sequence name. For example, the HCA(CO)N (*6, 7*) sequence involves coherence transfer from one amino acid residue to the next via the pathway $^{1}H \rightarrow {}^{13}C_{\alpha} \rightarrow {}^{13}C{=}O \rightarrow {}^{15}N$; however, the carbonyl $^{13}C$ shift is not encoded. In this study, a variety of HXY (where Y = $^{13}C$ and C = $^{31}P$) experiments are presented and used to characterize $^{31}P$-containing chain ends of PS. Since the pulse sequences employed in this study are based on the experiments for characterizing biomolecules, they are named using a similar convention.

### *Pulse Sequences*

All of the pulse sequences describe here make use of PFGs for coherence selection (*13*). The signals which must be detected are those from $^{1}H-{}^{13}C-X$ fragments, which only occur at the polymer chain end, and are ca. $1/10^{4}$ of the intensity of the $^{1}H$ resonances from the polymer main chain repeat units. The latter signals must be completely and reproducibly suppressed in order to obtain good quality 2D and 3D NMR spectra. Without the use of PFGs, both signal components are detected and digitized; phase cycling from multiple transients is used to cancel undesired signal components while the desired signals coadd. When using the phase cycling scheme alone, the receiver must be set to detect the large, undesired signal. Under these conditions, it is difficult to selectively detect the small differences between large signals, since the gain settings are not optimized for digitizing the weak signals. When PFGs are used, undesired signal components are destroyed before they reach the receiver system. Consequently, the receiver gain can be optimized for detection of the desired weak signal. Furthermore, the PFGs are much more effective than phase cycling for suppression of undesired coherences.

*HCAP.* The HCAP pulse sequence is analogous to the HNCA experiment used in structural biology; the most significant differences between these sequences are the substitutions of pulses at the $^{13}C$ and $^{31}P$ resonance frequencies for pulses at the $^{15}N$ and $^{13}C$ resonance frequencies in HNCA. In HCAP, the 3D correlations relate the shifts of $\alpha$-$^{13}C$ atoms with directly bound $^{1}H$ and $^{31}P$ atoms. While there are many ways to accomplish this, we have compared two methods which are illustrated by the pulse sequences in Fig. 1. The first of these methods is implemented with the pulse sequence in Fig. 1a. It involves INEPT type transfer from $^{1}H_{\alpha}$ to $^{13}C_{\alpha}$, $^{13}C$ chemical shift evolution during $t_1$ to encode the chemical shift of $^{13}C_{\alpha}$, followed by an HMQC type transfer during which three-spin multiple quantum (MQ) coherence develops among directly bound $^{1}H$, $^{13}C$, and $^{31}P$ atoms. This coherence in modulated by $\delta_{P}^{31}$ during $t_2$, then converted by to $^{13}C$ single quantum (SQ) coherence; this magnetization is then transferred from $^{13}C$ back to $^{1}H$ via a reverse INEPT sequence for $^{1}H$ detection during $t_3$. Because this experiment involves excitation of an MQ state involving directly bonded $^{1}H$, $^{13}C$, and $^{31}P$ atoms it will be called the MQ-HCAP experiment.

A second way of performing the HCP experiment involves sequential INEPT magnetization transfer steps from $^{1}H$ to $^{13}C_{\alpha}$, from $^{13}C_{\alpha}$ to $^{31}P$, $^{31}P$ chemical shift evolution during $t_1$, reverse INEPT transfer from $^{31}P$ back to $^{13}C_{\alpha}$, $^{13}C$ chemical shift evolution during $t_2$ to encode the chemical shift of $^{13}C_{\alpha}$, and finally reverse INEPT transfer from $^{13}C_{\alpha}$ to $^{1}H_{\alpha}$ for detection of protons during $t_3$. In this experiment, consecutive INEPT coherence transfers, between $^{1}H$ and $^{13}C$, and between $^{13}C$ and $^{31}P$, are performed. Therefore, this experiment contains SQ $^{31}P$ chemical shift evolution and is called the SQ-HCAP experiment. When uniform $^{13}C$ labeling is employed, a constant evolution time (CT = $\frac{1}{2J}$) is required during the $^{13}C$ chemical shift evolution period. When a CT chemical shift evolution period is employed in the SQ-HCAP experiment (Fig. 1c), one can optimize CT based on one-

bond $^{13}C-^{13}C$ couplings ($^{1}J_{CC}$) in order to accommodate enough increments in molecules having large one-bond $^{1}J_{XY}$ couplings between the X and Y nuclei (CT-HCAP). Alternatively, one can optimize CT based on the small long range $^{n}J_{XY}$ couplings to observe correlations between the chemical shifts of $^{31}P$ and either $\beta$- (CT-HCBP) or $\gamma$-$CH_n$ resonances.

All variations of the HCP experiment described here employ coherence selection PFGs. There are a large number of possibilities for placement of these gradient pulses. The sequences in Figs. 1a and 1b use PFG coherence selection between the resonances of $^{13}C$ and $^{1}H$, and the sequence in Fig. 1c uses coherence selection between $^{31}P$ and $^{1}H$. In each case, the ratio of the PFG pulse areas must satisfy the relationship $g_x \times t_{gX} \times \gamma_X = g_H \times t_{gH} \times \gamma_H$, where X is either $^{13}C$ or $^{31}P$, $g_X$ and $g_H$ are the gradient strength during the period when coherence resides on X and $^{1}H$, $t_{gX}$ and $t_{gH}$ are the times for the gradient pulses, and $\gamma_X$ and $\gamma_H$ are the magnetogyric ratios of the X and $^{1}H$ nuclei. In practice, coherence selection between $^{31}P$ and $^{1}H$, as in Fig. 1c, gives much better suppression of undesired signals. The sequences in Figs. 1a and 1b pass coherence components which precess at the $^{13}C$ resonance frequency during the g1 pulse and at the $^{1}H$ resonance frequency during the g2 pulse. Selective detection of $^{1}H-^{13}C$ correlations from groups bound to $^{31}P$ at the chain end is accomplished using phase cycling to cancel those signal components which are not influenced by coupling to $^{31}P$. The pulse sequence in Fig. 1c uses PFGs to select those signal components which precess at $^{31}P$ resonance frequency during g1 and at the $^{1}H$ resonance frequency during g2. In other words, the latter PFG coherence selection needs less help from phase cycling techniques. The PFG coherence selection has an important role in the success of these experiments. The signals that are observed in this work are often $10^{-6}$ times weaker than the signal originating from the main repeat unit of polystyrene; dynamic range, imperfect cancellation, and instrument instability cause tremendous artifacts when coherence is selected by phase cycling alone.

*$^{13}C-^{13}C$ Homonuclear Spin Locking Sequences.* Although detection of $^{13}C$ NMR resonances from polymer chain ends is a tremendous challenge at natural abundance, the detection of the signals becomes much easier when $^{13}C$ enrichment of the polymer backbone is performed. Enrichment permits the detection of signals originating from not only $\alpha$-$CH_n$ that are attached to chain end $^{31}P$ atoms, but also $CH_n$ that are few bonds away from the chain end $^{31}P$ atoms. One such way to detect these correlations is to optimize the delays in the pulse sequences shown in Fig. 1 for long-range $^{13}C-^{31}P$ couplings (e.g., CT-HCBP experiment). Another way is to introduce a $^{13}C$ spin-lock scheme in the experiment. The HCACO–TOCSY experiment (*24*) developed by Kay *et al.* has the potential to detect such correlations. However, the experiment correlates two $^{1}H$ chemical shifts much like the TOCSY experiment (*25*). Therefore, the broad $^{1}H$ resonances of polymers are not resolved. Additionally, $^{13}C$ chemical shift evolution occurs before the $^{13}C$ spin-locking takes place. With this configuration of the pulse sequence, we cannot take advantage of the large $^{13}C$ chemical shift dispersion that is often important for resolving resonances in polymer samples. Therefore, another pulse sequence is needed to satisfy these requirements.

*H(CA)P–CC-TOCSY.* In this study, two types of spin-locking 3D experiments were developed. The first sequence, which is shown in Fig. 2a, will be referred to as H(CA)P–CC-TOCSY. It involves sequential INEPT-type coherence transfer from $^{1}H$ to $^{13}C_\alpha$, then from $^{13}C_\alpha$ to $^{31}P$, followed by $^{31}P$ chemical shift evolution during the period $t_1$, reverse INEPT transfer from $^{31}P$ to $^{13}C_\alpha$, then $^{13}C$-TOCSY transfer from $^{13}C_\alpha$ down the backbone of the polymer. $^{13}C$ chemical shift evolution occurs during $t_2$ to encode information about the chemical shifts of the first few backbone carbons near the chain end. Finally, a reverse INEPT transfer from $^{13}C$ to $^{1}H$ permits selective detection during $t_3$ of $^{1}H$ resonances from protons directly bound to carbons which have received polarization during the spin lock part of the sequence. If a slice is selected at $f_1$ corresponding to the $^{31}P$ chemical shift of one of the chain ends, $^{13}C-^{1}H$ correlations will be observed for $CH_\alpha$, $CH_\beta$, $CH_\gamma$, and $CH_\delta$ backbone structure fragments. The biggest advantage of this experiment is that one can use the wide $^{13}C$ chemical shift range of the $^{13}C$ resonances that are part of the same spin system near the chain end.

*HCA(P)–CC-TOCSY.* There are circumstances when the $^{31}P$ chain end resonances are not well resolved. Under these circumstances it can be advantageous to use the $^{13}C_\alpha$ chemical shifts to disperse resonances along $f_1$. The second spin locking experiment is shown in Fig. 2b and will be referred to as the HCA(P)–CC-TOCSY experiment. It has a coherence transfer scheme identical to that of the H(CA)P–CC-TOCSY experiment, but differs by placing the $t_1$ chemical shift evolution period to encode the shift of the $\alpha$-$^{13}C$ instead of $^{31}P$ as in the first experiment. Therefore, these two experiments give similar spectra with $^{1}H-^{13}C$ correlation maps in $f_2/f_3$ dispersed along the $f_1$ axis based on either $^{31}P$ or $\alpha$-$^{13}C$ chemical shift of the chain ends.

*HCCH.* The last experiment used in this work is the CT-HCCH experiment shown in Fig. 3. This HCCH experiment was originally developed by Prestegard *et al.* (*21, 22*). Later, Saito and Rinaldi improved the HCCH experiment by making three modifications (*23*). The first modification is to reduce two sets of coherence-selection PFGs to only a pair of coherence selection PFGs. This reduction in the number of coherence-selection PFGs provides a twofold signal increase. The second point is to acquire two sets of FIDs with different signs for the last PFG: Complex Fourier transformation enables phase-sensitive detection in all three dimen-

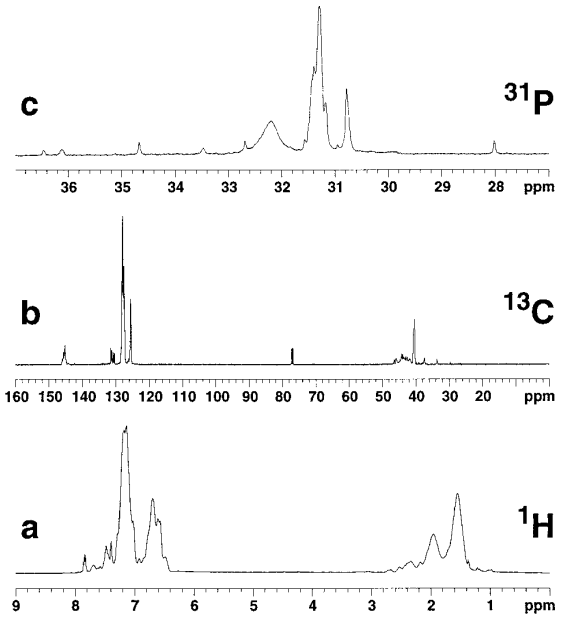


**FIG. 4.** 1D (a) $^{1}H$, (b) $^{13}C$, and (c) $^{31}P$ spectra of DPPR initiated polystyrene.

sions of the spectrum. The final improvement involves introduction of a CT evolution period (*26, 27*) in the $^{13}C$ chemical shift evolution time. Since samples used with this experiment are usually $^{13}C$ enriched, homonuclear couplings caused by the directly attached $^{13}C$ complicate the final spectrum; introduction of the CT $^{13}C$ evolution eliminates modulation from $^{13}C-^{13}C$ homonuclear coupling during $t_1$. In this experiment an INEPT transfer from $^{1}H$ to $^{13}C$ replaces the first 90° $^{13}C$ pulse in the INADEQUATE experiment (*28*). The experiment concludes with a reverse INEPT sequence to transfer polarization from $^{13}C$ to $^{1}H$ for detection. This $^{13}C$-DQ filtered experiment has the following chemical shift evolution: $\delta_{^{13}C\text{-SQ}}$ evolution during $t_1$, $\delta_{^{13}C\text{-DQ}}$ evolution during $t_2$, and $\delta_{^{1}H}$ evolution during $t_3$. Since this experiment involves excitation of $^{13}C$ DQ coherence, it is extremely difficult to perform on samples with $^{13}C$ at natural abundance where only 1 in $10^4$ molecules has adjacent, coupled $^{13}C$ nuclei. This DQ filtered HCCH experiment provides information much like the 2D-INADEQUATE. If a slice at the $f_3$ position of a proton is selected, that slice will contain the $^{13}C-^{13}C$ 2D-INADEQUATE correlations of the carbon bound to that proton. Therefore, when this experiment is combined with the spin-lock experiments, it is possible to make unambiguous chemical shift assignments for the first few carbons near the chains ends of PS.

*Polystyrene Spectra*

1D $^{1}H$, $^{13}C$, and $^{31}P$ NMR spectra of DPPR initiated PS are shown in Fig. 4. Expansions from the aliphatic region of the $^{1}H-^{13}C$ PFG–HMQC spectrum of this PS sample are shown in Fig. 5a. Despite the use of PFG and 2D NMR techniques, the resonances from the chain ends cannot be identified by inspection. Figure 5b shows a projection of the $f_2 f_3$ dimension from the 3D SQ-HCAP spectrum. This spectrum is equivalent to the HMQC spectrum, with the exception that only the correlations of resonances from $CH_n$ groups bound to $^{31}P$ are observed; the remainder of the C–H correlations are removed by PFG coherence selection. This additional level of filtering provides the simplification and improvement in spectral quality necessary to clearly detect the resonances from chain end groups. Several resonances are observed in Fig. 5b which are not seen in the PFG–HMQC spectrum in Fig. 5a. Despite the high field

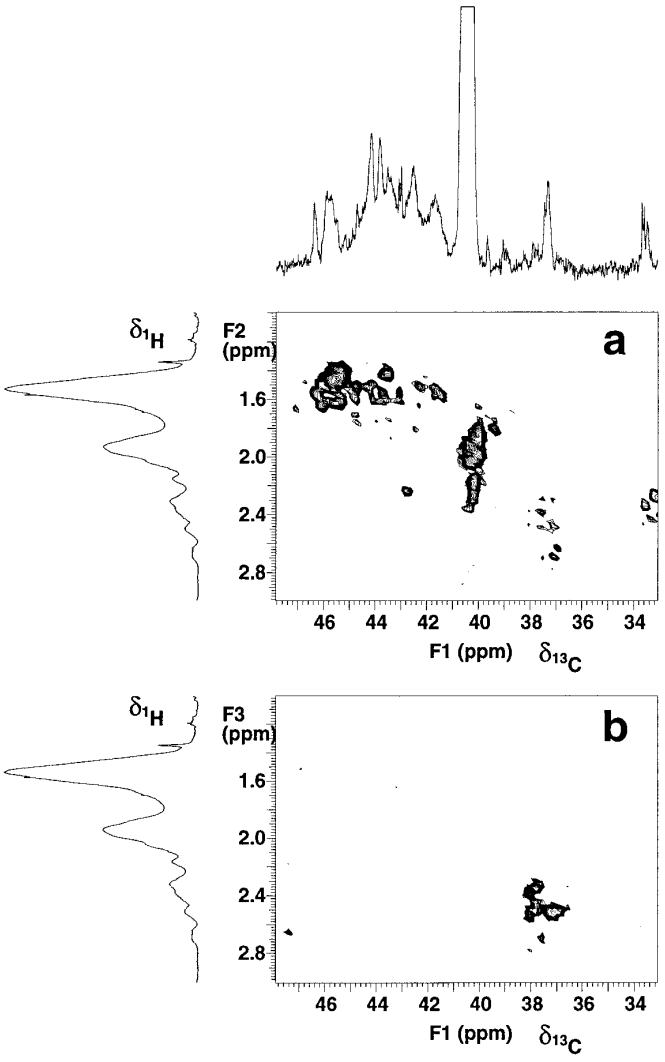


**FIG. 5.** Aliphatic regions from the 2D NMR spectra of polystyrene containing diphenylphosphinyl chain ends, with the 1D $^{1}H$ and $^{13}C$ spectra along the side and top axes, respectively: (a) $^{1}H-^{13}C$ PFG–HMQC; (b) corresponding region from the projection of $f_2 f_3$ plane from the 3D SQ-HCAP spectrum.

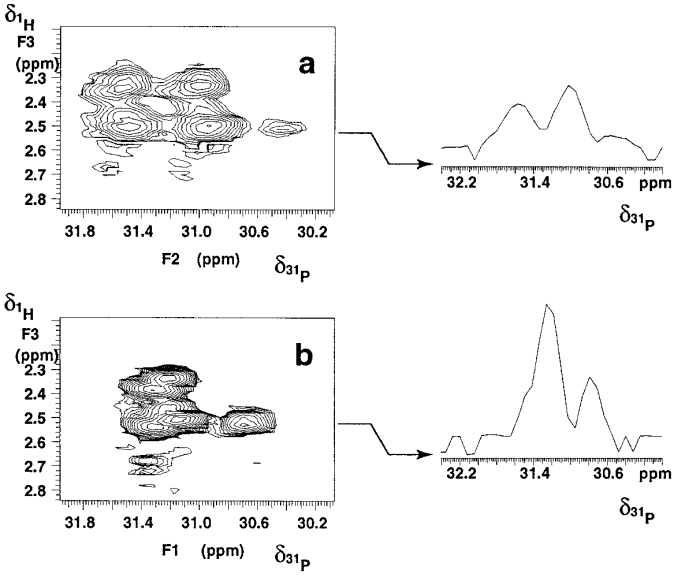


**FIG. 6.** $^{1}H-^{31}P$ projections from the HCP spectra of polystyrene containing diphenylphosphinyl chain ends, obtained from two different HCP experiments: (a) expansion of the $f_2 f_3$ projection from the MQ-HCAP spectrum; (b) corresponding region from the projection of $f_1 f_3$ plane from the 3D SQ-HCP spectrum. 1D traces from the indicated positions in the $^{1}H-^{31}P$ projections are plotted to the right of the 2D spectra to indicate the relative signal-to-noise levels in the two spectra.

(corresponding to a $^{1}H$ resonance frequency of 600 MHz) and the use of 2D NMR techniques, there is still considerable overlap of the resonances in the PFG–HMQC spectrum.

Figure 6 shows a comparison of two $^{1}H-^{31}P$ projections obtained with MQ- and SQ-HCAP experiments. Figure 6a is the projection obtained from the MQ-HCAP spectrum. In this spectrum, 146 Hz splittings were observed in the $^{31}P$ dimension which originate from $^{1}J_{HC}$ modulation during the $^{31}P$ chemical shift evolution period. Since three-spin coherence among $^{1}H$, $^{13}C$, and $^{31}P$ exists during this period in the MQ-HCAP experiment, the effect of $J$ coupling between $^{1}H$ and $^{13}C$ is evident in the resulting spectrum. The additional splitting in the MQ-HCAP spectrum makes it more difficult to interpret and causes problems from overlapping resonances. On the other hand, Fig. 6b, obtained with the SQ-HCAP sequence, shows less complex, better resolved, and more easily interpretable cross peak patterns. Because the SQ-HCAP experiment has only single spin coherence throughout the experiment, modulation by $J$ coupling between $^{1}H$ and $^{13}C$ does not occur during $t_1$, and coupling between $^{1}H/^{13}C$ and $^{31}P$ can be removed by the 180° refocusing pulse in the middle of the $^{31}P$ chemical shift evolution period, $t_1$. The absence of $J$ coupling between $^{1}H$ and $^{13}C$ also produces an improvement in signal-to-noise in the spectrum. Therefore, the SQ-HCAP pulse sequence provides a better quality spectrum when compared to the one obtained with the MQ-HCAP pulse sequence.

Figure 7 shows selected $f_2 f_3$ slices from the 3D SQ-HCAP spectrum at specific $^{31}P$ chemical shifts. The slices show well-resolved resonances from the chain ends, unobstructed by artifacts from the strong backbone resonances. From this spectrum, two classes of resonances ($\delta_{^{31}P} = 31.47$ and 31.31, Figs. 7a and 7b) are seen which are attributed to one chain end structure in which the diphenylphosphinyl group is bound to styrene methylene carbons (**1**); the second class of resonances ($\delta_{^{31}P} = 31.31$ and 30.66, Figs. 7c and 7d) are attributed to chain end structures in which the diphenylphosphinyl group is bound to styrene methine carbons. These assignments can be made by inspection, based on the fact that phosphorus is bound to a methylene carbon with chemically nonequivalent protons in **1;** therefore, slices from these groups show correlations between one $^{13}C$ and two $^{1}H$ resonances. In Figs. 7c and 7d, phosphorus is bonded to a methine carbon which exhibits one bond coupling to only a single proton. Consequently, slices from these groups would show correlations between single $^{13}C$ and $^{1}H$ resonances. Some of the additional fine structure in these slices is due to the variety of stereoisomers possible, since each styrene unit bears a stereogenic center (e.g., the slice in Figure 7b contains two pair of peaks from the different methylene carbons). Additionally, signal intensity bleeds into adjacent slices because of the limited digital resolution in the $f_1$ ($^{31}P$ chemical shift) dimension. For example, the slice in Fig. 7b, from a $CH_2$ group, reveals a trace of the pair of $CH_2$ resonances from the slice in Fig. 7a.

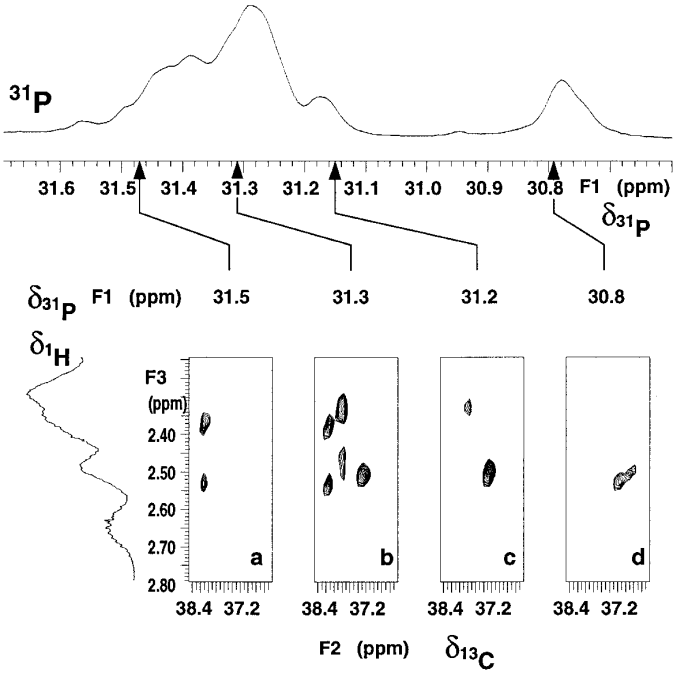


**FIG. 7.** Selected $f_2 f_3$ slices along the $^{31}P$ chemical shift axis, from the SQ-HCAP spectrum of polystyrene containing diphenylphosphinyl chain ends.

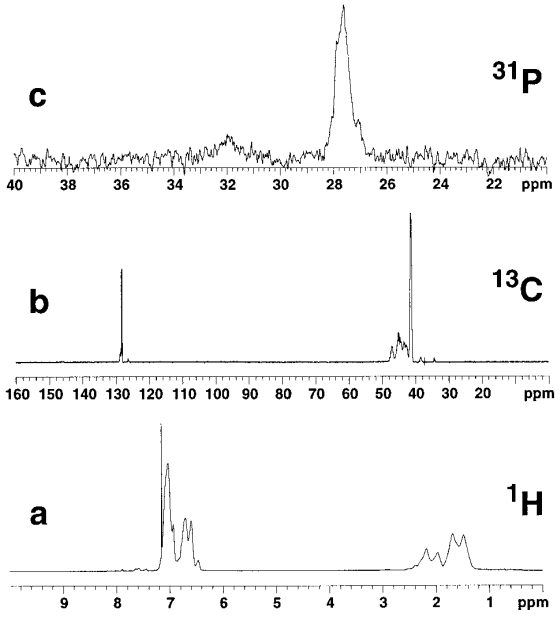


**FIG. 8.** 1D (a) $^{1}$H, (b) $^{13}$C, and (c) $^{31}$P spectra of DPPR initiated PS with 99% $^{13}$C enrichment of the backbone CH and $CH_2$ resonances.

*Poly($\alpha$,$\beta$-$^{13}C_2$-styrene)*

The HCP experiments selectively detect signals originating from $CH_n$ groups directly bonded to $^{31}$P and filters out all other signals, thus providing the identity of the first carbon in the polymer chain. In order to understand the initiation step in polymerization, it is necessary to obtain chemical shift information of not only the $CH_n$ groups directly bonded to the $^{31}$P nucleus ($C_\alpha$), but also those originating from a few repeat units away from the $^{31}$P nucleus (i.e., $C_\beta$, $C_\gamma$, $C_\delta$, $C_\epsilon$. . .). Detecting signals based on the long-range $J_{CP}$ or performing $^{13}C-{}^{13}C$ relay type experiments are extremely difficult with natural abundance $^{13}$C because of the low concentration of the chain ends. Therefore, PS labeled with $^{13}$C along the backbone CH and $CH_2$ carbons was prepared via initiation of $\alpha$,$\beta$-$^{13}C_2$-styrene polymerization with DPPR in order to facilitate detection and correlation of resonances from the structures formed at early stages of this polymerization.

1D $^{1}$H, $^{13}$C, and $^{31}$P NMR spectra of this labeled PS are shown in Fig. 8. The aliphatic peaks in the $^{1}$H spectrum exhibit splitting caused by $J_{HC}$ due to the $^{13}$C enrichment, and the $^{31}$P spectrum exhibits broad, weak signals because of numerous one-bond and multiple bond $J_{CP}$ couplings. The signals in the aliphatic region of the $^{13}$C spectrum are much stronger than those shown in Fig. 4. In $^{13}$C enriched material, the presence of $^{13}C-{}^{13}C$ homonuclear couplings interfere the total evolution of $^{13}$C chemical shift and heteronuclear couplings, $J_{CP}$. Because the precession from homonuclear couplings during the indirectly detected $^{13}$C chemical shift evolution period is not refocused, additional splitting is observed in the spectrum. The effect caused by the heteronuclear $J_{CP}$ and homonuclear $J_{CC}$ couplings in this case are of the same order, for example, $J_{CP}$ = 60 Hz and $J_{CC}$ = 35 Hz, and thus the effect caused by the $J_{CC}$ during the standard chemical shift evolution distorts the resulting spectrum. To overcome this problem, a CT chemical shift evolution in the $^{13}$C dimension is necessary for the indirect detection of $^{13}$C chemical shift evolution. During the CT evolution, the duration of the $^{13}$C chemical shift evolution and refocusing delay of heteronuclear couplings are combined and are kept constant. The net effect is that homonuclear couplings do not modulate the signal during this delay. Therefore, the CT $^{13}$C chemical shift evolution is essential for observing clean spectra from samples with $^{13}$C enrichment.

Figure 9a shows the $f_2 f_3$ projection of the CT-HCAP spectrum. This spectrum displays signals from $CH_n$ directly bonded to $^{31}$P much like the SQ-HCAP spectrum in Fig. 9b. Despite the $^{13}$C enrichment, this CT-HCAP spectrum of the PS shows resonances originating from the carbons ($C_\alpha$) which are similar to the resonances in the spectrum of the unlabeled sample, which is shown in Fig. 5b. The $f_2 f_3$ projection of the CT-HCBP spectrum (Fig. 9b) shows three groups of cross peaks. The first group of cross peaks (Fig. 9b, region 1) are also found in the CT-HCAP spectrum. Those $^{1}H-{}^{13}C$ correlations ($\delta_{^1H}$ = 2.2, $\delta_{^{13}C}$ = 38.5) originate from $CH_n$ groups directly bonded to $^{31}$P atoms at the chain end. The second group of cross peaks (Fig. 9b, region 2) correlate the $^{1}$H resonances between 2.7 and 3.3 ppm with the $^{13}$C resonances around 38.5 ppm. The third group of cross peaks (Fig. 9b, region 3) correlate the $^{13}$C resonances between 47 and 43 ppm and the resonances of the two nonequivalent $^{1}$H atoms. Looking at the $f_2 f_3$ projection of the H(CA)P–CC-TOCSY spectrum (Fig. 9c), a fourth group of correlations to the $^{13}$C resonances around 41.5 ppm (Fig. 9c, region 4) are found. Although weak, those four peaks can also be found in the $f_2 f_3$ projection of the HCA(P)–CC-TOCSY spectrum shown in Fig. 9d. The second, third, and fourth groups of cross peaks originate from carbons two to four bonds away from the chain end $^{31}$P nucleus. It is important to assign these resonances in order to determine the chain end structures.

Figure 10 contains 1D traces from the 3D NMR spectra showing a comparison of signal intensities observed with the three different pulse sequences which can be used to obtain long-range structure correlations. The CT-HCBP spectrum contains the strongest signal when the $^{13}$C has two- or three-bond $J$ coupling to the chain end $^{31}$P atom. However, this experiment does not produce correlations with $^{13}$C atoms four bonds away from the chain end $^{31}$P atom. Under these circumstances, the long-range couplings are too small to permit coherence transfer before relaxation effects reduce the transverse magnetization. If the sensitivity for detection of the correlations four bonds away is required, the H(CA)P–CC-TOCSY experiment provides the strongest

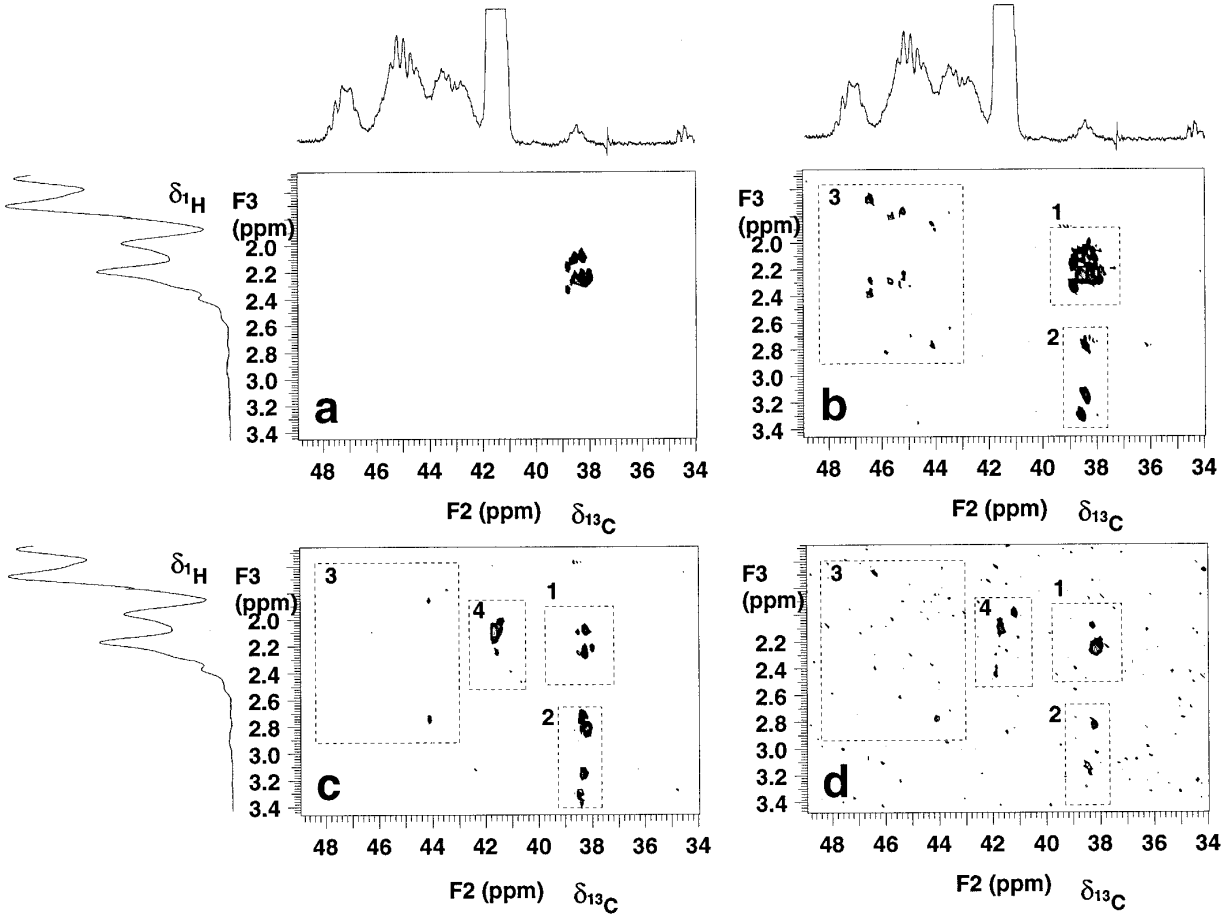


**FIG. 9.** The $f_2 f_3$ projection of the HCP spectra of DPPR initiated poly($\alpha,\beta$-$^{13}C_2$-styrene) observed with (a) CT-HCAP, (b) CT-HCBP, (c) H(CA)P–CC-TOCSY, and (d) HCA(P)–CC-TOCSY pulse sequences. Corresponding regions from the $^1$H and $^{13}$C spectra are plotted along the side and top axes, respectively.

signal intensity. Although the HCA(P)–CC-TOCSY experiment has the poorest sensitivity of the three experiments, this spectrum provided the best spectral dispersion of the resonances from the PS structures of interest in this work. Under certain circumstances the relative spectral dispersion of the X and $^{13}$C nuclei might supersede sensitivity considerations in determining which of the two spin locking sequence to use.

Figure 11 illustrates the combined use of these sequences to obtain complete characterization of one of the PS chain end structures. This figure contains selected slices from the four different experiments at chemical shifts corresponding to the resonances of chain end **1.** The resonance assignments start with the identification of the $^1$H and $^{13}$C resonances from the methylene group bound to one of the $^{31}$P atoms. The $f_1 f_3$ slice from the CT-HCAP spectrum (Fig. 11a) at $f_2 = \delta_{C\alpha}$ identifies the resonances from one of the $^{31}$P–$^{13}CH_2$ fragments.

The second step in the characterization procedure is to identify the next $CH_n$ fragment in the chain. This can be accomplished by looking for $^1$H/$^{13}$C correlations from CH-$\beta$ at the shift of $^{31}$P, or it can be accomplished by searching for the $^1$H resonances from the $H_\alpha$ methylene protons in an $f_2 f_3$ slice from the HCCH spectrum at $^{13}$C SQ chemical shift of $C_\alpha$ (Fig. 11b). From this spectrum, connectivity between $C_\alpha$ and $C_\beta$ is proven, enabling identification of the $C_\beta$ and $H_\beta$ resonances. Since the CT-HCCH experiment is not a $^{31}$P filtered experiment, additional confirmation that the resonance attributed to $C_\beta$ is in fact $\beta$ to the chain end $^{31}$P atoms can be useful. To accomplish this, the $C_\beta$ resonance was used to identify an $f_1 f_3$ slice from the H(CA)P–CC-TOCSY (Fig. 11c) and HCA(P)–CC-TOCSY (Fig. 11d) spectra. These slices also contain C–H correlations for the $\alpha$-$CH_2$. The four spectra give a self-consistent set of resonance assignments. In practice, only two or three of these spectra would be needed to provide reliable resonance assignments.

Resonance assignments for the next monomer unit in the chain derive from the known positions of the $\beta$-CH $^1$H and $^{13}$C resonances, which can then used to select the appropriate $f_2 f_3$ slice of the CT-HCCH spectrum (Fig. 11e) and the

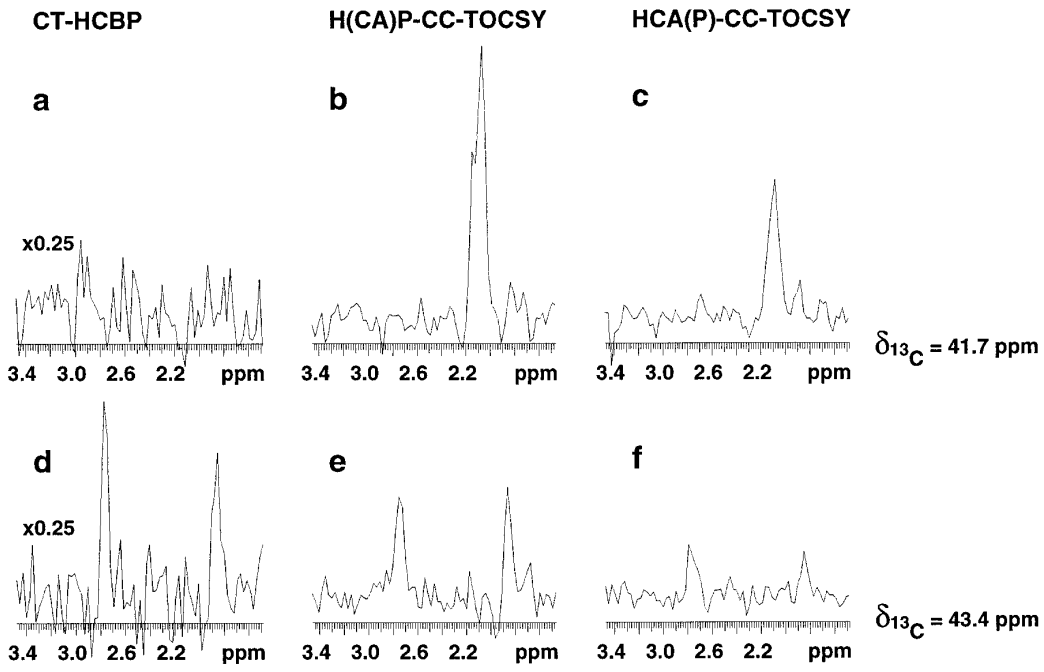


**FIG. 10.** Comparison of signal intensities in the 1D traces obtained with four different 3D experiments. These traces were all extracted from slices of the 3D spectra which correspond to the chain end whose $^{31}$P resonance is at 27.5 ppm. The slices in (a,b,c) are at $\delta^{13}_{C}$ = 41.7 ppm and the slices in (d,e, f ) are at $\delta^{13}_{C}$ = 43.4 ppm. The three pulse sequences used were (a,d) CT-HCBP, (b,e) H(CA)P–CC-TOCSY, and (c, f ) HCA(P)–CC-TOCSY. All spectra except the CT-HCBP spectra, whose vertical scale was reduced fourfold, were plotted at the same vertical scale.

$f_1 f_3$ slices from the H(CA)P–CC-TOCSY (Fig. 11f) and HCA(P)–CC-TOCSY (Fig. 11g) spectra. These slices all contain correlations which relate the $\beta$-CH $^1$H and $^{13}$C resonances with the $\gamma$-$CH_2$ $^1$H and $^{13}$C resonances. The CT-HCCH spectrum is not very clean because it contains many other signals from the rest of the polymer chain. However,

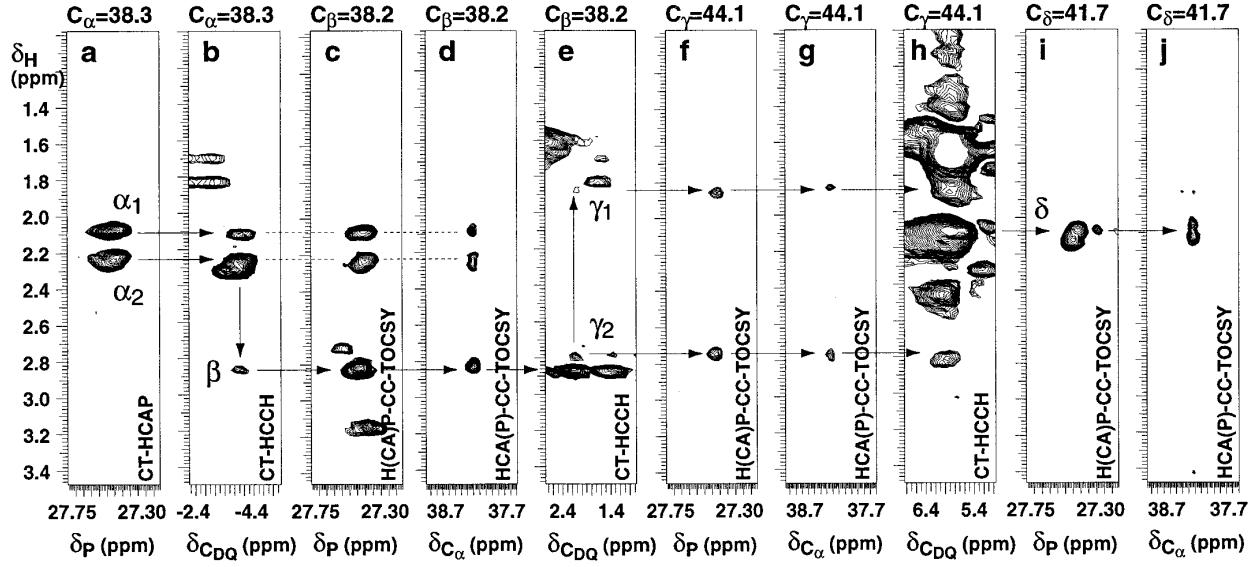


**FIG. 11.** Slices from a variety of 3D-NMR spectra of DPPR initiated poly($\alpha$,$\beta$-$^{13}C_2$-styrene). Spectrum (a) was obtained with the CT-HCAP pulse sequence; (b,e,h) were obtained with the CT-HCCH pulse sequence; (c, f ,i) were obtained with the H(CA)P-CC-TOCSY pulse sequence; and (d,g, j) were obtained with the HCA(P)–CC-TOCSY pulse sequence. Arrows indicate the connectivities from $C_\alpha$ through $C_\delta$. The slices are each labeled at the top with $^{13}$C SQ chemical shift of that slice, and the carbon number responsible for that slice.

**TABLE 1**
**Chemical Shift Assignments for the Chain End Structure 1 of DPPR Initiated PS**

| Nucleus | $^{31}$P | $^{13}$C | $^{1}$H |
|---|---|---|---|
| $\alpha$ | 27.4–27.7 | 38.3 | 2.08, 2.24 |
| $\beta$ | — | 38.2 | 2.82 |
| $\gamma$ | — | 44.1 | 1.86, 2.72 |
| $\delta$ | — | 41.7 | 2.09 |

the H(CA)P–CC-TOCSY and HCA(P)–CC-TOCSY spectra unequivocally link the $\gamma$-$CH_2$ $^{1}$H and $^{13}$C resonances to the $^{31}$P and $\alpha$-$CH_2$ resonances of the chain end structure **1.**

A similar procedure is used to identify the $\delta$-CH resonances from the CT-HCCH, H(CA)P–CC-TOCSY, and HCA(P)–CC-TOCSY spectra (Figs. 11h–j). The slice from the CT-HCCH spectrum (Fig. 11h) is particularly complex because of overlap with the very intense CH resonances from the polymer main chain repeat units. Although longer $^{13}$C spin locking times could in principle provide spectra which permit resonance assignments for backbone carbons of the third monomer unit in the chain, in practice they also result in significant attenuation of all the signals in the spectrum. Consequently, longer spin locking times provided spectra in which very few resonances were detectable.

Table 1 shows a summary of the chemical shift assignments of the resonances due to **1** at the chain end of this polymer.

## CONCLUSIONS

In this work, it is demonstrated that the use 3D HCP experiments provides spectra of good quality such that resonances of minor structures can be detected in the presence of much larger signals from the polymer main chain repeat unit, enabling one to make unambiguous assignments of the resonances originating from polymer chain end structures which are present in very low concentrations. Three-dimensional chemical shift correlation experiments provide enormous spectral dispersion and the unique correlation of three nuclei provides definitive structure information. When coherences from the right combination of nuclei are chosen, one can disperse overlapping resonances and obtain simple chemical shift correlation maps. The X-nucleus filtration experiments greatly simplify the resulting spectra, thus enabling chemical shift assignments to be made.

In order to detect the trace components in the presence of huge signals, PFG coherence selection techniques are essential. Residual $t_1$ noise caused by incomplete suppression of undesired signals is usually at or above the intensities of the signals of interest when phase cycling alone is used for coherence selection. Additionally, dynamic range may cause problems in detection of resonances originating from trace structures. When triple resonance and PFG are combined, one can detect signals originating from trace structures in polymeric materials without resorting to isotopic enrichment. When the enrichment is possible, it provides more detailed chemical shift information.

The series of 3D NMR techniques described here can be used together to extract a phenomenal amount of detailed structural information about polymer chain ends, defects, and branch points, inorganic polymers, and organometallic compounds. The HCX experiments have already provided useful information from fluorinated polymers (*29*), polycarbosilanes (*30*), and organometallic star branched polymers. The chemical shift assignments will help to characterize stereochemistry and monomer sequence distribution in polymers, and elucidate initiation and termination reactions. Although the examples described here involve polymer characterization, the pulse sequences can be directly applied to other organic structures containing three mutually coupled nuclei. Immediate applications in organometallic chemistry are envisioned.

## ACKNOWLEDGMENTS

We gratefully acknowledge the Kresge Foundation and all the donors to the Kresge Foundation Challenge Grant at the University of Akron for supporting the purchase of the 600-MHz NMR spectrometer. We thank the NSF (DMR-9310642 and DMR-9617477) and the State of Ohio Board of Regents Academic Challenge and Research Challenge Grants for supporting this research. We also thank H. J. Harwood, R. Medsker, and F. Wyzgoski for samples of polystyrene and $^{13}$C-labeled polystyrene.

## REFERENCES

1. D. H. Solomon, P. Cacioli, and G. Moad, *Pure Appl. Chem.* **57,** 985 (1985).
2. J. Kristina, G. Moad, and D. H. Solomon, *Eur. Polym. J.* **25,** 767 (1989).
3. T. V. Holland, S. D. Goodrich, M. Guo, H. J. Harwood, T. Saito, and P. L. Rinaldi, *Polymer Reprints* **36,** 91 (1995).
4. P. L. Rinaldi and N. J. Baldwin, *J. Am. Chem. Soc.* **104,** 5791 (1982).
5. P. L. Rinaldi and N. J. Baldwin, *J. Am. Chem. Soc.* **105,** 7523 (1983).
6. M. Ikura, L. E. Kay, and A. Bax, *Biochemistry* **29,** 4659 (1990).
7. L. E. Kay, M. Ikura, R. Tschudin, and A. Bax, *J. Magn. Reson.* **89,** 496 (1990).
8. S. Berger and P. Bast, *Magn. Reson. Chem.* **31,** 1021 (1993).
9. S. Berger, *J. Magn. Reson. Ser. A* **105,** 95 (1993).
10. H. A. Heus, S. S. Wijmenga, F. J. M. van de Ven, and C. W. Hilbers, *J. Am. Chem. Soc.* **116,** 4983 (1994).
11. J. P. Marino, H. Schwalbe, C. Anklin, W. Bermel, D. M. Crothers, and C. Griesinger, *J. Am. Chem. Soc.* **116,** 6472 (1994).
12. J. Cavanagh, W. J. Fairbrother, A. G. Palmer III, and N. J. Skelton, ''*Protein NMR Spectroscopy Principles and Practice,*'' Academic Press, New York (1996).
13. R. E. Hurd, *J. Magn. Reson.* **87,** 422 (1990).

*14.* P. L. Rinaldi, D. G. Ray III, V. E. Litman, and P. A. Keifer, *Polym. Int.* **36,** 177 (1995).

*15.* R. E. Medsker, Ph.D. Dissertation, University of Akron, Akron, Ohio (1992).

*16.* A. J. Shaka, P. B. Barker, and R. Freeman, *J. Magn. Reson.* **64,** 547 (1985).

*17.* T. Fujiwara, T. Anai, N. Kurihara, and K. Nagayama, *J. Magn. Reson. Ser. A* **104,** 103 (1993).

*18.* T. Fujiwara and K. Nagayama, *J. Magn. Reson.* **77,** 53 (1988).

*19.* A. J. Shaka, C. J. Lee, and A. Pines, *J. Magn. Reson.* **77,** 274 (1988).

*20.* A. J. Shaka, J. Keeler, and R. Freeman, *J. Magn. Reson.* **53,** 313 (1983).

*21.* Y. Q. Gosser, K. P. Howard, and J. H. Prestegard, *J. Magn. Reson. Ser. B* **101,** 126 (1993).

*22.* J. C. Tolman, K. P. Howard, and J. H. Prestegard, *J. Magn. Reson. Ser. B* **102,** 137 (1993).

*23.* T. Saito and P. L. Rinaldi, *J. Magn. Reson. Ser. A* **118,** 136 (1996).

*24.* L. E. Kay, M. Ikura, A. A. Grey, and D. R. Muhandiram, *J. Magn. Reson.* **99,** 652 (1992).

*25.* L. Braunschweiler and R. R. Ernst, *J. Magn. Reson.* **53,** 521 (1983).

*26.* A. Bax and R. Freeman, *J. Magn. Reson.* **44,** 542 (1981).

*27.* J. Santoro and G. C. King, *J. Magn. Reson.* **97,** 202 (1992).

*28.* A. Bax, R. Freeman, and S. P. Kempsell, *J. Am. Chem. Soc.* **102,** 4849 (1980).

*29.* L. Li and P. L. Rinaldi, *Macromolecules* **29,** 4808 (1996).

*30.* M. Chai, T. Saito, Z. Pi, C. Tessier, and P. L. Rinaldi, *Macromolecules* **30,** 1240 (1997).

*31.* D. J. States, R. A. Haberkorn, and D. J. Ruben, *J. Magn. Reson.* **48,** 286 (1982).

*32.* J. Keeler and D. Neuhaus, *J. Magn. Reson.* **63,** 454 (1985).